

Journal of Materials Chemistry A

Accepted Manuscript



This is an *Accepted Manuscript*, which has been through the Royal Society of Chemistry peer review process and has been accepted for publication.

Accepted Manuscripts are published online shortly after acceptance, before technical editing, formatting and proof reading. Using this free service, authors can make their results available to the community, in citable form, before we publish the edited article. We will replace this *Accepted Manuscript* with the edited and formatted *Advance Article* as soon as it is available.

You can find more information about *Accepted Manuscripts* in the [Information for Authors](#).

Please note that technical editing may introduce minor changes to the text and/or graphics, which may alter content. The journal's standard [Terms & Conditions](#) and the [Ethical guidelines](#) still apply. In no event shall the Royal Society of Chemistry be held responsible for any errors or omissions in this *Accepted Manuscript* or any consequences arising from the use of any information it contains.

Cite this: DOI: 10.1039/c0xx00000x

PAPER

www.rsc.org/xxxxxx

Cadmium removal in waste water by nanostructured TiO₂ particles

Ruhua Zha,^a Reddeppa Nadimicherla,^a Xin Guo*^a

Received (in XXX, XXX) Xth XXXXXXXXX 20XX, Accepted Xth XXXXXXXXX 20XX

DOI: 10.1039/b000000x

Nanostructured TiO₂ dandelions and spherical flowers with an anatase structure were synthesized by a solvothermal method, and characterized by means of XRD, SEM, TEM, BET, FT-IR, XPS and TG. The specific surface areas of the dandelions and spherical flowers were determined by BET to be 226 and 172 m² g⁻¹, respectively. The maximum monolayer adsorption capacities of Cd(II) for the dandelions and spherical flowers were found to be 396 and 282 mg g⁻¹, respectively, and both nanostructured TiO₂ particles could be repeatedly used without any remarkable loss in the adsorption capacity. The FT-IR, XPS and TG-MS analyses indicated that the Cd(II) adsorption was mainly ascribed to the hydroxyl groups on the TiO₂ surfaces. Both nanostructured particles exhibited great potential for the removal of Cd(II) from wastewater in engineering practices.

Introduction

Heavy metal pollution is a common environmental problem, and anthropogenic wastewater containing heavy metals is the main source of water pollution in developing countries.¹ Particularly, cadmium is a toxin of environmental concern. The impact for non-cancer concerns includes kidney, liver, and lung damage.² Many technologies have been developed to remove the heavy metal ions in soil and water. Physical adsorption is a convenient technique, which is the most cost-effective for the heavy metal removal due to many advantages, such as easy operation, low secondary pollution, etc. Many adsorbents such as mesoporous silica³ and metal oxides⁴ have been used for the removal of heavy metal ions. Recent research works on the toxic heavy metal removal from water has focused on the preparation of materials with increased capacities for the targeted metal ions. Different types of substrates, including polymers,⁴⁻⁷ amorphous silica⁸ and clays⁹ have been used to prepare functionalized materials with heavy metal complexing groups. Nevertheless, some of these materials suffer from inherent problems, e.g. low removal capacity, long equilibrium time, mechanical and thermal instability, etc.

The advent of nanotechnology has given immense opportunities for the fabrication of desired nanostructures with large surface-to-volume ratios (and hence excellent chemical reactivities) and unique functionalities to treat pollutants. Therefore, the synthesis of inorganic nanomaterials with controllable size and shape has attracted more and more attention due to their specific structures and potential applications. Nanostructures TiO₂ is chemical inert and nontoxic,¹⁰ and has been demonstrated to have unique ability in the removal of a variety of inorganic/organic contaminants in waste water and air. A variety of nanostructured TiO₂ materials have been prepared,

including spheres,^{11,12,13} nanofibers,¹⁴ nanowires^{15,16} and nanotubes.^{17,18} The synthetic methods include anodic oxidation,^{19,20} CVD,²¹ sol-gel,^{22,23} etc. Mainly three strategies can be applied to obtain complex nanostructures:²⁴⁻³¹ template-based synthesis, in which soft or hard templates are used as structure-directing agents,²⁶⁻²⁸ oriented attachment, by which the kirkendall effect can lead to the formation of many new nanostructures,^{25,32,33} and induced anisotropic growth by using specific capping agents.²⁵ Hydrothermal method, as a wet chemical method, has attracted particular attention in recent years due to its advantages, e.g. the simplicity of operation, low energy consumption and potential large-scale industrialization.³⁴ However, particles are obtained by the hydrothermal method usually have smooth surfaces and lack of sharp edges and corners, resulting in less sites for reaction on the surfaces. Therefore, there is of great importance to modify the hydrothermal method to obtain ideal particles with specific function. For example, Lou and coworkers reported a novel sandwich-structured TiO₂-Pt-graphene ternary hybrid electrocatalysts with high efficiency and stability by a modified hydrothermal methods.^{35,36}

In this work, we successfully synthesized nanostructured anatase TiO₂ with unusual morphologies, namely dandelion and spherical flower. The synthesis of the nanostructured TiO₂ particles with two different morphologies were achieved through controlling the alcoholysis rate of TiF₄, the aggregation of morphology control agent, pressure, and pH value of the reaction solution. We found that the surface of anatase TiO₂, especially the dandelions, have a large number of OH groups, which can provide efficient chelating sites to coordinate with heavy metal ions. The Cd(II) adsorption experiment demonstrated that both particles showed good performances in the waste water treatment. The dandelions exhibited enhanced surface area compared with that of spherical flowers, and an excellent efficiency for the

Cd(II) adsorption in the water treatment.

2. Experimental

2.1. Preparation of nanostructured TiO₂ particles

2.1.1. Dandelions

In a typical dandelion synthesis procedure, 0.50 g of TiF₄ (Alfa Aesar, 98%) was added to 30 ml absolute ethanol (Alfa Aesar, AR) solution during strong stirring for 20 minutes (bottle A), and 0.7 g LiBr (Alfa Aesar, AR) and 0.8 g CO(NH₂)₂ (Alfa Aesar, AR) were poured into 15 ml distilled water during vigorous stirring for 60 minutes to form a mixed solution (bottle B). Then bottle B was added into bottle A and again stirred for another 15 minutes, the resulting solution was then transferred into a 50 ml Teflon-lined stainless steel autoclave and treated solvothermally at 180 °C for 30 h, and afterwards cooled down to room temperature. The final products were centrifuged, and rinsed with distilled water and ethanol several times to remove any fluoride and bromide remains, and finally dried in oven at 60 °C overnight.

2.1.2. Spherical flowers

The spherical flower nanostructures were prepared by an one-pot solvothermal reaction method. 0.3 g TiF₄ was added to 65 ml absolute ethanol solution during strong stirring for 60 minutes (bottle A) and 0.5 g NaF and 2 g CO(NH₂)₂ were poured into 10 ml distilled water, then allowed to homogeneous mixing (bottle B) under stirring for 30 minutes. Bottle B was then added into bottle A, and again stirred for 3 h to form a mixed solution. The resulting solution was transferred into a 100 ml autoclave and treated solvothermally at 180 °C for 48 h, and finally cooled down to room temperature. The further procedures were the same as those of the dandelions.

2.2. Characterization of nanostructured TiO₂ particles

Power X-ray diffraction (XRD) spectra were measured by means of a Philips diffractometer (PW 3050) operated at 40 kV and 40 mA with Cu-K α monochromatic radiation, at the Bragg's angle range from 20 to 80°. The nanostructures of the spherical flowers and dandelions were observed by scanning electron microscopy (SEM, Nova NanoSEM450). Transmission electron microscopy (TEM) investigations were carried out using a JEOL 2100F microscopy. Nitrogen adsorption and desorption isotherms were determined by nitrogen physisorption at -196 °C with a Micromeritics ASAP 2020 analyzer. The pore size distribution (PSD) was calculated via a non-local density functional theory (NLDFT) method by using nitrogen adsorption data and assuming a slit pore model.^{37,38} The chemical characteristics of the adsorbents were analyzed by a Bruker VERTEX 70 Fourier transform infrared spectrometer (FT-IR). X-ray Photoelectron Spectroscopy (XPS) measurements were performed on a VG MultiLab 2000 system with a monochromatic Al K α X-ray source (ThermoVG Scientific). The binding energy values were calibrated with the C 1s signal at 284.5 eV. The thermal stability of the adsorbents was investigated using a thermogravimetric analysis (TG) with a NETZSCH Instruments' high resolution STA 449F3 thermogravimetric analyzer, which was purged with nitrogen at a flow rate of 50ml/min from 50 to 800 °C. And a

quadrupole mass spectrometer, model QMS 403, was linked to the thermogravimetric apparatus to measure the evolved water vapour in this work.

2.3. Batch adsorption

A batch-wise process was employed to study the adsorption of Cd(II) from aqueous solutions on the dandelions and spherical flowers. All the adsorption batch experiments were performed at 25 °C. In the adsorption isotherm studies, batch experiments were carried out at pH 5.0 with various initial Cd(II) concentrations (40, 60, 80, 100, 140, 180 and 200 mg L⁻¹). The mixtures were centrifuged at 18000 rev/min. for 30 minutes, and the residual concentration of Cd(II) was determined by atomic adsorption spectrometer (AAS, Varian Spectra AA 55). An aliquot of this solution (1 ml) was diluted to a final volume of 50 ml with distilled water, and the unbound Cd(II) ions present in this solution were exposed to AAS analysis. All the adsorption experiments were performed in triplicate and the mean values were used in the data analysis. Consecutive adsorption-desorption cycles were performed. The adsorbed Cd(II) were eluted with different concentrations of HCl (0.05, 0.1, 0.5, 1.0, 2.0 mol·L⁻¹). The eluted adsorbents (dandelions and spherical flowers) were washed thoroughly with distilled water to remove any residual desorption reagents and then placed into the Cd(II) solution for the subsequent adsorption-desorption cycles.

3. Results and Discussion

3.1. Characterization of dandelions and spherical flowers

All nanostructured particles are crystallized and have an anatase structure, as evidenced from the XRD patterns (Figure 1).

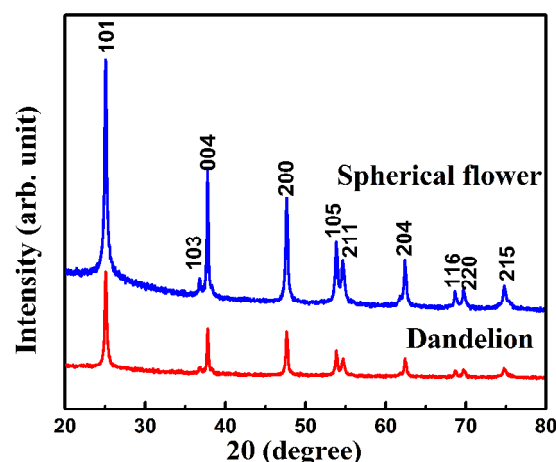


Fig. 1 XRD patterns of TiO₂ dandelions and spherical flowers.

According to Figures 2A to C, the dandelions are ~5 μm in diameter, and consisted of numerous uniform nanorods with a typical diameter of 70 nm, and a length of 200-250 nm. The distance of about 0.35 nm between adjacent lattice fringes (Figure 2D) can be well assigned to the *d* spacing value of (101) planes in the anatase structure. The dandelions were plausibly formed by a three-step process.³⁹ Firstly, TiO₂ nano-particles were quickly built in the solution and spontaneously aggregated to form large microspheres to minimize the surface area. Afterwards, the crystal growth process transferred to a kinetically controlled

process and then crystal growth was initiated preferentially from the active nano-particles on the surfaces of the microspheres. In the presence of Br^- as morphology-controlling agent, these clusters served as seeds of the subsequent growth along the c axis, by which the dandelion nanostructure was thus formed.

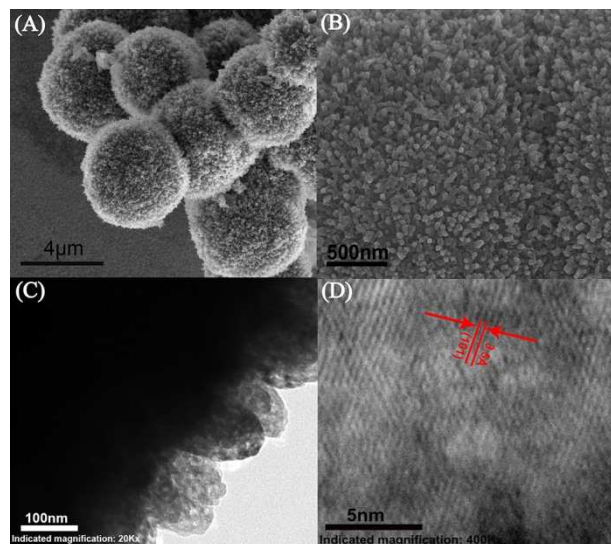


Fig. 2 (A) SEM image of TiO₂ dandelion, (B) magnified view of the surface, (C) TEM image of nanorods and (D) high resolution TEM image of dandelions.

As shown in Figures 3A to C, the spherical flowers are consisted of multi-layer nanosheets. The nanosheets are single crystalline, and the lattice fringes can also be assigned to the d spacing value of (101) planes in the anatase structure. The spherical flowers were also plausibly formed in three steps.⁴⁰ At the beginning of the reaction, TiO₂ nano-particles were produced in the solution. Then these nano-particles were quickly aggregated into nanosheets. Afterwards the TiO₂ nanosheets spontaneously generated a dissolution-recrystallization process by the Ostwald ripening. As the reaction time continues, in the present of F^- as etching agent, the spherical flower structure was formed with a bunch of nanosheets standing on the surfaces.

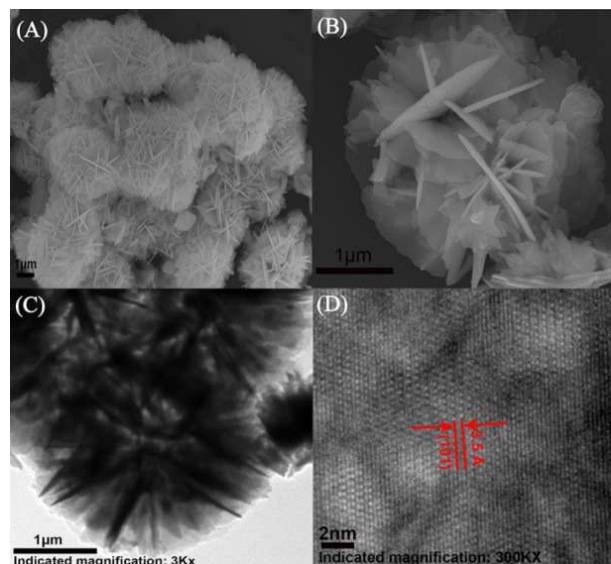


Fig. 3 (A, B) SEM images, (C) TEM image of spherical flowers, and (D) high

resolution TEM image of nanosheet.

The BET curves of the dandelions and spherical flowers are depicted in Figure 4, which describes nitrogen adsorption-desorption isotherms and their corresponding pore size distributions. Both dandelions and spherical flowers show type II isotherms and the BET surface area were found to be 226 and 172 m² g⁻¹, respectively, and their average pore sizes are 4.1 and 4.5 nm, respectively. The narrow pore size distribution for the dandelions is consistent with their uniform morphology.

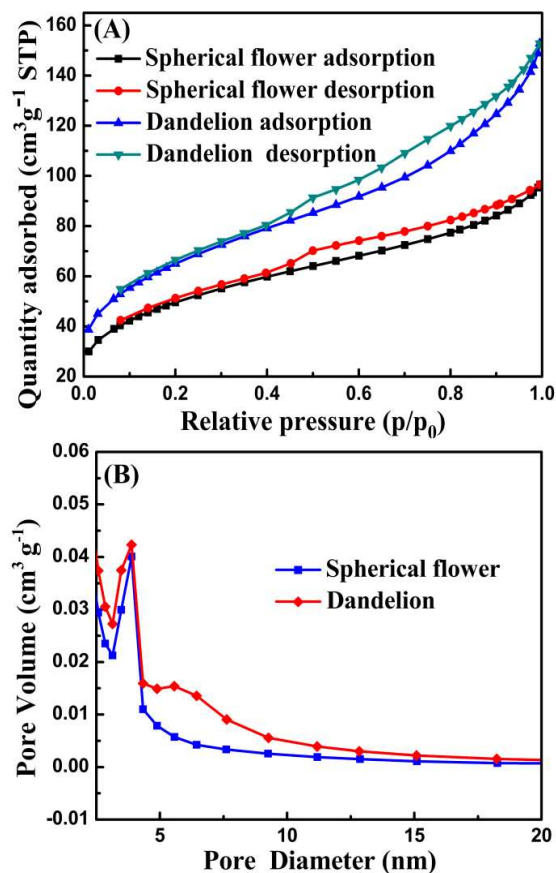


Fig. 4 (A) Nitrogen adsorption-desorption isotherms, and (B) corresponding pore size distributions of the dandelions and spherical flowers.

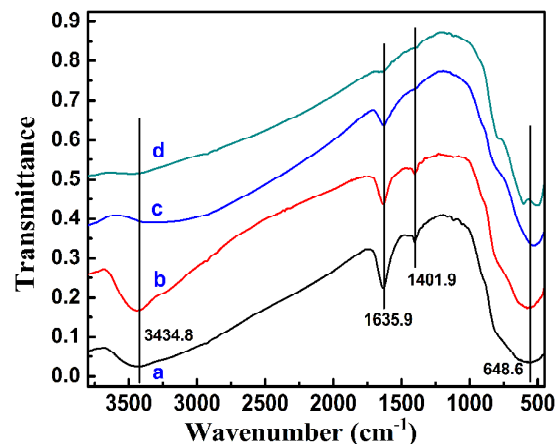


Fig. 5 FT-IR spectra of (a) dandelions annealed at 70°C, (b) spherical flowers annealed at 70°C, (c) dandelions annealed at 180°C and (d) spherical flowers annealed at 180°C.

spherical flowers annealed at 180 °C.

The FT-IR spectra of the dandelions and spherical flowers are shown in Figure 5. The FT-IR spectra are almost the same for the dandelions and spherical flowers. The broad peaks observed at 3434.8 cm^{-1} correspond to the stretching vibration of surface hydroxyls and adsorbed water,⁴¹ the peaks at 1635.9 cm^{-1} are due to the bending vibration of Ti-OH, the bands at about 1401.9 cm^{-1} are related to the bending vibration of Ti-O-Ti, and the bands at below 800 cm^{-1} are due to the Ti-O stretching vibration. These results are consistent with the those reported by Shabalin.⁴²⁻⁴⁴ The broad peaks observed at 3434.8 cm^{-1} disappeared after annealing at 180 °C, demonstrating that the adsorbed water in the surface of dandelions and spherical flowers was removed by heating, but the peaks at 1635.9 cm^{-1} corresponding to the bending vibration of Ti-OH still existed, which benefits the adsorption of Cd(II).

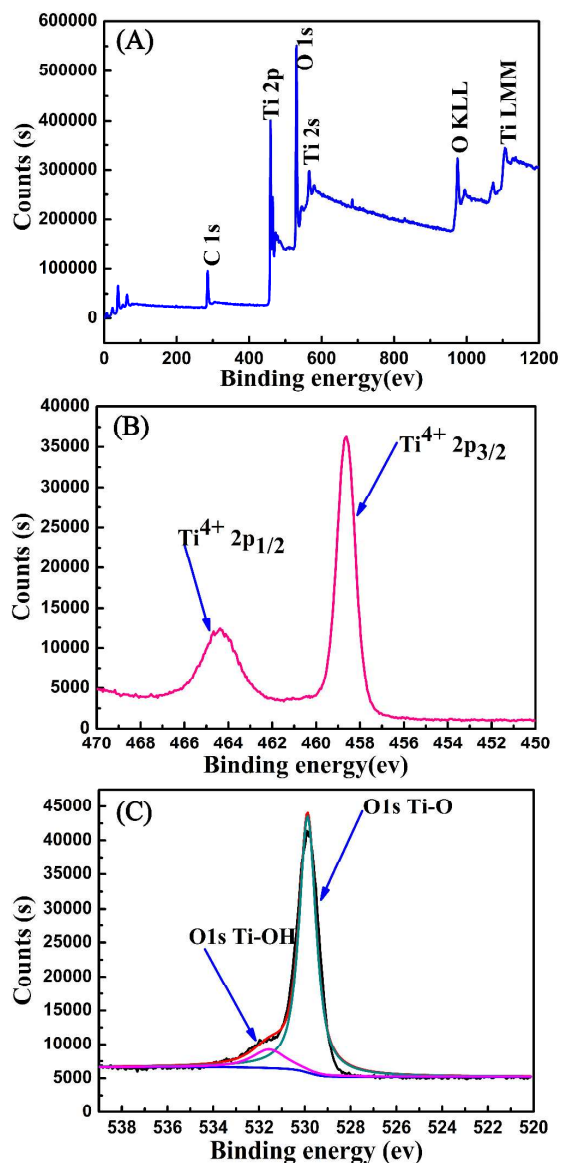


Fig. 6 XPS spectra of TiO_2 dandelions: (A) wide-survey spectrum, (B) Ti 2p core level and (C) O 1s core level.

To obtain an in depth understanding of the composition and chemical state of the TiO_2 particles, the samples were

investigated by XPS, and the spectra of the dandelions are given in Figure 6. Figure 6A shows the survey wide-scan spectrum, the O 1s and Ti 2p peaks were obtained at binding energies of 529 and 459 eV, respectively, and the Ti LMM and O KLL Auger peaks were also obtained at binding energies of 1106 and 975 eV, respectively. Figure 6B shows the Ti 2p core level spectrum, which consists of two distinct Ti 2p_{1/2} and Ti 2p_{3/2} photopeaks with the binding energies of 464.5 and 458.7 eV, respectively. The peaks are not very broad and no shoulder peaks were observed, being consistent with the observations by Siemensmeyer and Schultze.⁴⁵ The binding energy at 458.7 eV indicates the presence of Ti^{4+} . The XPS spectrum of O 1s is also composed of two peaks (Figure 6C), the first strong peak at a low binding energy of 529.7 eV corresponds to bulk oxygen bonded with titanium (Ti-O), whereas the second shoulder peak at 531.5 eV corresponds to the hydroxyl group (Ti-OH). The XPS results are consistent with those of FT-IR.

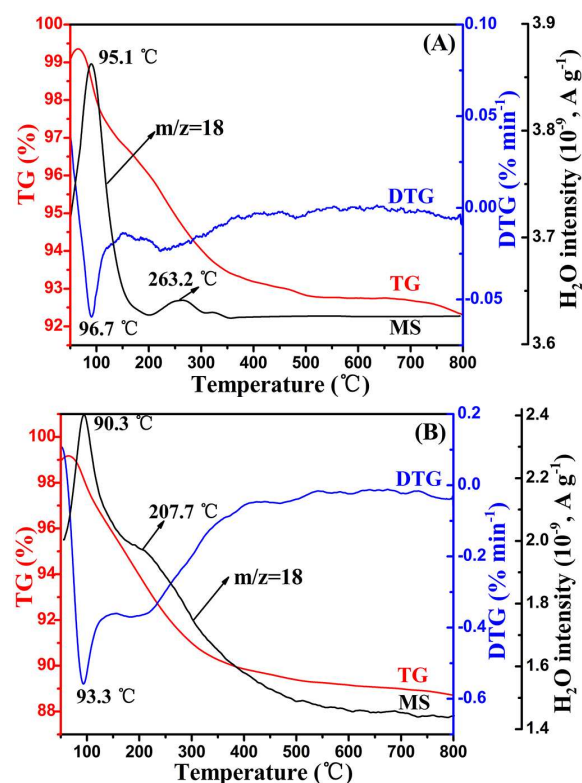


Fig. 7 Evolution curves of H_2O during pyrolysis of (A) dandelions and (B) spherical flowers.

The dandelions or spherical flowers were further investigated by TG-MS. The measured gas in this work was water vapour. Figure 7A shows the evolution curves of H_2O ($m/z=18$) during pyrolysis of the TiO_2 dandelions. The peak at below 95.1 °C reflects the moisture of the samples. At temperature above 200 °C, the signal was attributed to the dehydration reaction of the Ti-OH groups.⁴⁶ Figure 7B shows the evolution curves of H_2O ($m/z=18$) during pyrolysis of the spherical flowers. The peak at below 90.3 °C reflects the moisture of the samples. At temperature above 200 °C, only a faint signal, a wider peak was detected, indicating the weaker dehydration reaction of the Ti-OH groups in the spherical flowers, as compared with that of the dandelions. The FT-IR, XPS and TG-

MS results are consistent with each other, they all demonstrate the existence of the Ti-OH groups.

3.2. Adsorption studies

Removal efficiency R (%) and the amount of Cd(II) q_t (mg g^{-1}) at any time t , and the amount of Cd(II) q_e (mg g^{-1}) at equilibrium, taken up by the dandelions and spherical flowers from aqueous solution at 25 °C was determined using the equations:

$$R = \frac{C_0 - C_t}{C_0} \times 100, \quad (1)$$

$$q_t = \frac{(C_0 - C_t)V}{m}, \quad (2)$$

$$q_e = \frac{(C_0 - C_e)V}{m}, \quad (3)$$

where C_0 is the initial concentration of Cd(II) (mg L^{-1}), C_t the Cd(II) solution concentration at any time t (mg L^{-1}), C_e the Cd(II) solution concentration at equilibrium (mg L^{-1}), V the solution volume (L) and m the adsorbent mass (g).

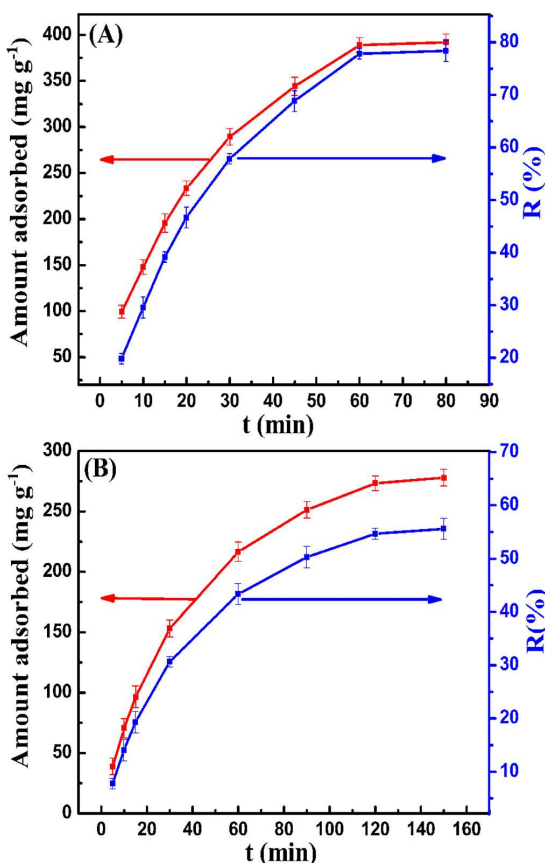


Fig. 8 Effect of contact time on adsorption of Cd(II) by (A) dandelions and (B) spherical flowers (initial Cd(II) concentration = 100 mg L^{-1} , initial pH = 5, temperature = 25 °C, contact time = 80 min for dandelions and 150 min for spherical flowers).

3.2.1. Effect of contact time

The effect of contact time on the adsorption of Cd(II) by the

dandelions and spherical flowers was investigated to determine the time taken for the adsorption equilibrium. The results are illustrated in Figure 8. It is evident that the adsorption capacity of Cd(II) by the dandelions (Figure 8A) increased sharply within the first 30 minutes for the initial concentration of 100 mg L^{-1} . With the further increase of contact time, the adsorption of Cd(II) made a slow approach towards equilibrium until 80 minutes. After 80 min, almost 80% Cd(II) was removed. Therefore, 80 minutes of contact time is considered to be appropriate for the equilibrium adsorption of Cd(II) by the dandelions.

The uptake of Cd(II) by the spherical flowers (Figure 8B) was slightly slower than that of the dandelions. As can be seen from Figure 8B, 150 minutes of contact time is appropriate for the equilibrium adsorption of Cd(II). However, only about 50% Cd(II) was removed by the spherical flowers after 150 min. The difference in Cd(II) adsorption between the dandelions and spherical flowers was probably attributed to the different numbers of available active adsorption sites. As the contact time increased, the adsorption sites gradually became exhausted, and later the uptake rate decreased on account of the slow pore diffusion of Cd(II) into the bulk of the dandelions and spherical flowers.

3.2.2. Effect of initial pH

The external pH influences the activity of functional groups. The surface charges of adsorbents can be modified by changing pH of the solution. The effect of initial pH (1.0–6.0) on the adsorption of Cd(II) by the dandelions and spherical flowers is shown in Figure 9. It can be clearly observed that at any pH, the uptake of Cd(II) by the dandelions is much greater than that of the spherical flowers. The adsorption of Cd(II) by both dandelions and spherical flowers experienced similarly rapid rise at initial pH of 1.0–3.0, followed by a slow increase at pH 3.0–5.0 to an approximately constant at pH 5.0–6.0. The optimum adsorption capacities of Cd(II) were found in the pH range of 5.0–6.0. With an increase of pH from 1.0 to 6.0, the uptake of Cd(II) by the dandelions increased from 95.4 to 392.0 mg g^{-1} , and from 62.6 to 278 mg g^{-1} by the spherical flowers at an initial concentration of 100 mg L^{-1} .

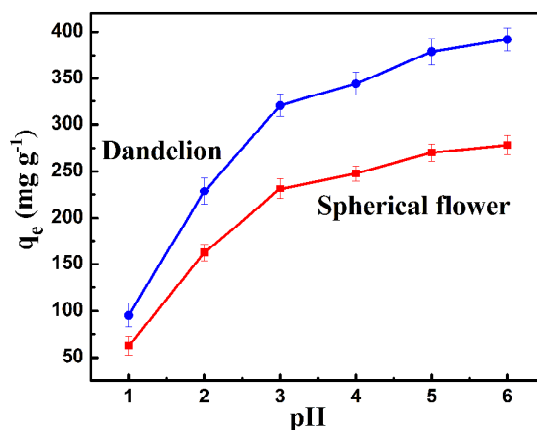


Fig. 9 Effect of initial pH value on adsorption of Cd(II) by dandelions and spherical flowers (initial Cd(II) concentration = 100 mg L^{-1} , temperature = 25 °C, contact time = 80 min for dandelions and 150 min for spherical flowers).

In the acidic solution, the possible sites on the dandelions and spherical flowers for specific adsorption stem from the H^+ ions in hydroxy groups.⁴⁷ When the adsorption occurs, divalent Cd(II) displaces one proton from hydroxy groups to form $\text{Cd}(\text{OH})^+$ species adsorbed. With the increase of pH value, the adsorbed $\text{Cd}(\text{OH})^+$ species continue to displace one proton to

form soluble $\text{Cd}(\text{OH})_2$. The decrease in the adsorption capacities of $\text{Cd}(\text{II})$ at the pH value smaller than 6.0 can be attributed to protonation of the hydroxy groups on the dandelions and spherical flowers. At higher pH values (>6.0), the concentration of soluble product of $\text{Cd}(\text{OH})_2$ is exceeded, therefore, $\text{Cd}(\text{II})$ is removed from the solution by adsorption as well as by precipitation. Thus to correlate $\text{Cd}(\text{II})$ removal with adsorption (ion exchange), an optimum initial pH of 5.0 was chosen to perform all subsequent adsorption experiments. At this pH, the ion exchange and complex formation process are the major mechanism for the removal of metal ions from solution.⁴⁷ The removal capacities of $\text{Cd}(\text{II})$ by two kinds of adsorbents increased in the order of dandelion $>$ spherical flower.

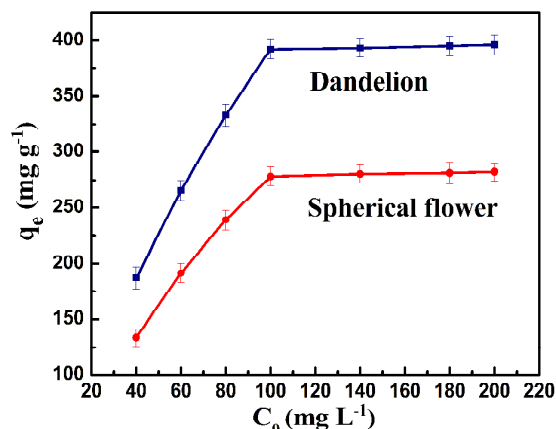


Fig. 10 Effect of initial $\text{Cd}(\text{II})$ concentration on adsorption of $\text{Cd}(\text{II})$ by dandelions and spherical flowers (initial pH = 5, temperature = 25 °C, contact time = 80 min for dandelions and 150 min for spherical flowers).

3.2.3. Effect of initial $\text{Cd}(\text{II})$ concentration

The effect of initial $\text{Cd}(\text{II})$ concentration on the adsorption capacities by the dandelions and spherical flowers are depicted in Figure 10. It can be seen that the adsorption capacity by the dandelions at equilibrium increased sharply as the initial $\text{Cd}(\text{II})$ concentration increased from 40 to 100 mg L^{-1} , and became nearly constant as the $\text{Cd}(\text{II})$ concentration further increased. The isotherm profile is similar for the spherical flowers, but the profile for the dandelions is much steeper. When the initial $\text{Cd}(\text{II})$ concentration increased from 40 to 200 mg L^{-1} , the adsorption capacity of the dandelions increased from 187 to 396 mg g^{-1} , and

from 134 to 282 mg g^{-1} for the spherical flowers. The maximum adsorption capacity of the dandelions for $\text{Cd}(\text{II})$ was found to be 396 mg g^{-1} , compared with 282 mg g^{-1} for the spherical flowers. At low $\text{Cd}(\text{II})$ concentrations $<$ 100 mg L^{-1} , the adsorption sites were unsaturated, resulting in unsaturated $\text{Cd}(\text{II})$ adsorption. However, at higher $\text{Cd}(\text{II})$ concentrations (100–200 mg L^{-1}), the adsorption sites would be insufficient for the adsorption reaction. The surfaces of TiO_2 particles can provide copious numbers of active adsorption sites, and facilitate $\text{Cd}(\text{II})$ transportation in the adsorption process. The different morphologies of the dandelions and spherical flowers and their different specific surface areas (226 and 172 $\text{m}^2 \text{g}^{-1}$, respectively), contribute to the different numbers of active adsorption sites.

3.3. Adsorption mechanism and kinetics

Figure 11 is the schematic diagram for the adsorption of $\text{Cd}(\text{II})$ by the dandelions and spherical flowers; the bonding of $\text{Cd}(\text{II})$ by the OH groups plays a key role. The BET specific surface areas and the pore volumes of the dandelions are 226 $\text{cm}^2 \text{g}^{-1}$ and 0.236 $\text{cm}^3 \text{g}^{-1}$, respectively, which are higher than those of the spherical flowers by a factor of 1.31 and 1.58, respectively. The obvious increase in surface areas and porosity of the dandelions could be ascribed to the unique morphology. The uniform channels on the surface of the TiO_2 particles can provide copious active adsorption sites, and facilitate $\text{Cd}(\text{II})$ transportation in the adsorption process.

To understand the adsorption mechanisms, the uptake rate of $\text{Cd}(\text{II})$ at an initial concentration of 40, 60, 80, 100, 140, 180 and 200 mg L^{-1} were analyzed by two kinetic models, i.e., pseudo-first-order and pseudo-second-order kinetic, respectively. The pseudo-first-order kinetic model is expressed in the following linearized form⁴⁸

$$\log(q_e - q_t) = \log q_e - \frac{k_1}{2.303} t, \quad (4)$$

where q_e and q_t (mg g^{-1}) are the amount of $\text{Cd}(\text{II})$ adsorbed at equilibrium and an elapsed time t , respectively, t (min) contact time, and k_1 (min^{-1}) pseudo-first-order rate constant. k_1 and q_e can be computed from the slope and intercept of the plot of $\log(q_e - q_t)$ versus t .

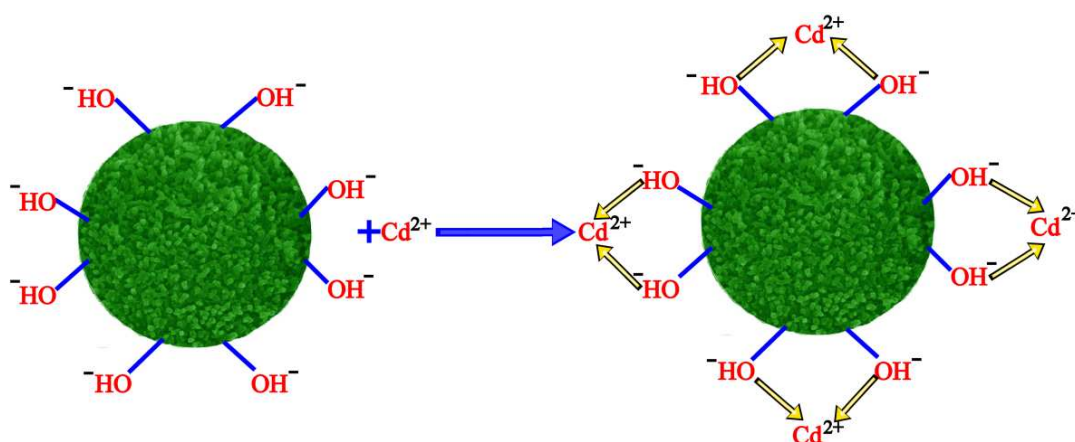


Fig. 11 Schematic diagram of the adsorption of $\text{Cd}(\text{II})$ by nanostructured TiO_2 particles.

The pseudo-second-order kinetic model is described by the following equation⁴⁸

$$\frac{t}{q_e} = \frac{1}{k_2 q_e^2} + \frac{1}{q_e} t, \quad (5)$$

where k_2 ($\text{g mg}^{-1} \text{min}^{-1}$) is pseudo-second-order rate constant. The values of k_2 and q_e can be calculated from the slope and intercept of the plot of t/q_t versus t .

The parameters of two kinetic models are calculated and listed in Table 1. The pseudo-first-order model shows poor fitting to the experimental data with low correlation coefficients ($r^2 = 0.885$ and 0.866 for the dandelions and spherical flowers, respectively). In contrast, the pseudo-second-order model provides excellent correlation coefficients ($r^2 > 0.99$). Hence it can be concluded that the adsorption of Cd(II) onto the dandelions and spherical flowers is more suited for the pseudo-second-order kinetic model, indicating that the rate controlling step might be chemisorptions.⁴⁹ The reasonably fast kinetics reflects good accessibility of the binding sites of the dandelions and spherical flowers to Cd(II). The enhanced adsorption rates have significant advantage in terms of time and space over the conventional techniques.

The difference in Cd(II) adsorption between the dandelions and spherical flowers can be attributed to the different numbers of available active adsorption sites. Because the dandelions possess a larger surface areas, they may expectedly provide abundant active sites that can coordinate with Cd(II). In addition, high pore volumes allows for the fast diffusion of Cd(II) into the pores of the dandelions. All these characteristics synergistically harvest the improvement of adsorption capacities of the dandelions for Cd(II).

3.4. Adsorption isotherms

The adsorption isotherms of Cd(II) are correlated either by the Langmuir or Freundlich models. The Langmuir model assumes that the monolayer surface adsorption occurs on specific homogeneous sites and no interaction exists between the adsorbed pollutants. The equation for this model can be written as

follows:

$$\frac{C_e}{q_e} = \frac{1}{K_L Q} + \frac{1}{Q} C_e, \quad (6)$$

where C_e (mg L^{-1}) is the equilibrium metal ion concentration, q_e (mg g^{-1}) the amount of metal ion adsorbed at equilibrium, Q (mg g^{-1}) the maximum adsorption capacity of the adsorbent, and K_L (L mg^{-1}) the Langmuir constant related to the free energy of adsorption.

The Freundlich isotherm⁴⁸ as an empirical equation describing heterogeneous surface adsorption is usually expressed as:

$$\log q_e = \log K_F + \frac{1}{n} \log C_e, \quad (7)$$

where K_F (mg g^{-1}) is the Freundlich constant related to the adsorption capacity of the adsorbent, and n is the heterogeneity factor indicating the adsorption intensity of the adsorbent.

Table 2 lists the constants and correlation coefficients involved in the two isotherm models. It is found that the Langmuir model exhibits good fit to the adsorption data for Cd(II) with high correlation coefficients ($r^2 = 0.999$ and 0.921 for the dandelions and spherical flowers, respectively). However, the Freundlich model represents a poor fit to the data for both adsorbents. The Langmuir adsorption behaviour for both adsorbents implies the existence of homogeneous active sites in the dandelions and spherical flowers and the monolayer adsorption of Cd(II) on the adsorbents. Moreover, the monolayer maximum adsorption capacities were calculated from the Langmuir isotherm to be 404.8 and 137.7 mg g^{-1} for the dandelions and spherical flowers, respectively. Compared with other adsorbents in the previous works (listed in table 3), it is apparent that the dandelions in this work have much higher adsorption capacities for Cd(II); therefore, the dandelions are very promising for the effective removal of Cd(II) in environmental remediation.

Table 1 Kinetic parameters of Cd(II) adsorption (25 °C, pH = 5.0)

Sample	q_e (exp)	Pseudo-first-order			Pseudo-second-order		
		K_1 (min^{-1})	q_e (cal)	r^2	k_2 ($\text{g mg}^{-1} \text{min}^{-1}$)	q_e (cal)	r^2
Dandelion	396	7.53×10^{-2}	623.7	0.885	8.45×10^{-5}	512.8	0.996
Spherical flower	282	3.16×10^{-2}	312.6	0.866	6.88×10^{-5}	359.7	0.998

Table 2 Fitting parameters of Langmuir and Freundlich adsorption isotherms for Cd(II) adsorption (25 °C, pH = 5.0)

Samples	Langmuir			Freundlich		
	q_m ($\text{mg} \cdot \text{g}^{-1}$)	K_L ($\text{L} \cdot \text{mg}^{-1}$)	r^2	$1/n$	K_F	r^2
Dandelion	404.8	0.3890	0.999	0.406	185.5	0.806
Spherical flower	137.7	0.006035	0.921	0.329	80.7	0.759

Table 3 Maximum Cd(II) adsorption capacities by various adsorbents

Adsorbents	Maximum capacities (mg g^{-1})	Reference
chinese loess	9.37	[1]
Multiwalled carbon nanotubes	10.86	[50]
Oxidized corncob	55.20	[51]
Titanate nanotubes	238.61	[49]
Titanate dandelions	404.8	This work

3.5. Desorption and regeneration studies

For an effective recycling process, adsorbed metal ions should be easily desorbed under suitable conditions without destroying the adsorbent material.⁵² In this work, desorption experiments were carried out using HCl as the desorption agent. The data in Figure 12 show the elution rate of Cd(II) as a function of HCl concentration; it is apparent that 0.5 mol L^{-1} HCl gives the best desorption result.

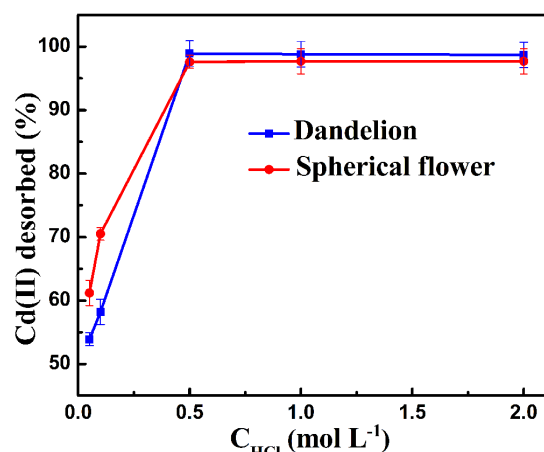


Fig. 12 Effect of HCl concentration (as the eluent) on the recovery of Cd(II) desorbed from dandelions and spherical flowers.

To demonstrate the reusability of the adsorbents, consecutive adsorption-desorption cycles were performed; the results are shown in Figure 13. After three adsorption-desorption cycles, the adsorption capacities of the dandelions and spherical flowers became 368 (Figure 13A) and 260 mg L^{-1} (Figure 13B), respectively, indicating that the removal and recovery capacities of the dandelions and spherical flowers did not degrade noticeably. Therefore, the nanostructured TiO_2 particles could be repeatedly used without any remarkable loss in the adsorption capacity.

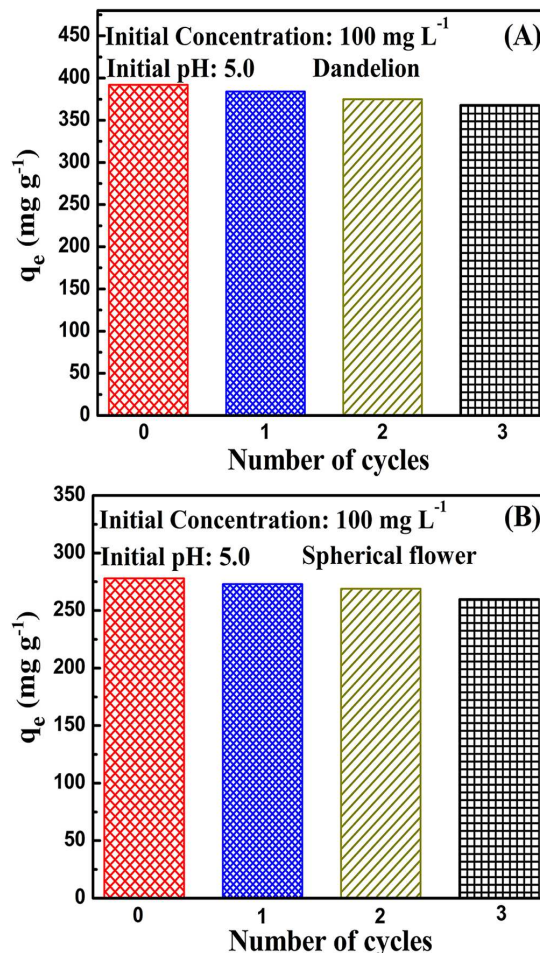


Fig. 13 Cd(II) adsorption-desorption cycles with 0.5 mol L^{-1} HCl as desorption agent.

4. Conclusions

Nanostructured TiO_2 dandelions and spherical flowers with specific surface areas of 226 and $172 \text{ m}^2 \text{ g}^{-1}$, respectively, were prepared by a solvothermal method. The maximum amount of the Cd(II) adsorption was achieved in the pH range of 5.0 – 6.0 , and the maximum monolayer adsorption capacity of Cd(II) by the dandelions was determined to be 396 mg g^{-1} . The adsorption kinetics was pretty fast, which could be completed within 80 minutes. More importantly, after three adsorption-desorption cycles, the adsorption capacity of the dandelions did not show any obvious degradation. The hydroxyl groups on the surfaces of the dandelions were responsible for Cd(II) adsorption. Hence, the nanostructured TiO_2 dandelions exhibit great potential for the removal of Cd(II) from contaminated water in engineering practices.

Notes and references

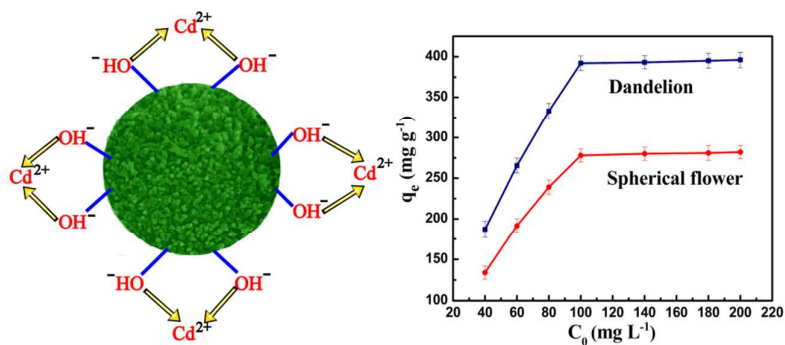
^a Laboratory of Solid State Ionics, School of Materials Science and Engineering, Huazhong University of Science and Technology, Wuhan 430074, P.R. China

* Author to whom correspondence should be addressed. Tel: +86-27-87559804; Fax: +86-27-87559804; E-mail: xguo@hust.edu.cn

- 1 Y. Wang, X. W. Tang, Y. M. Chen, L. T. Zhan, Z. Z. Li, and Q. Tang, *J. Hazard. Mater.*, 2009, **172**, 30-37.
- 2 M. P. Waalkes and S. Rehm, *J. Toxicol. Environ. Health.*, 1994, **43**, 251-269.
- 3 S. R. Li, X. A. Jiao and H. Q. Yang, *Langmuir*, 2013, **29**, 1228-1237.
- 4 R. R. Navarro, K. Sumi and M. Matsumura, *Water Res.*, 1999, **33**, 2037-2044.
- 5 Y. L. Chen, B. C. Pan, S. J. Zhang, H. Y. Li, L. Lv and W. M. Zhang, *J. Hazard. Mater.*, 2011, **190**, 1037-1044.
- 6 Y. L. Chen, B. C. Pan, H. Y. Li, W. M. Zhang, L. Lv, and J. Wu, *Environ. Sci. Technol.*, 2010, **44**, 3508-3513.
- 7 R. R. Navarro, K. Sumi, N. Fujii and M. Matsumura, *Water Res.*, 1996, **30**, 2488-2494.
- 8 P. K. Jal, S. Patel and B. K. Mishra, *Talanta*, 2004, **62**, 1005-1028.
- 9 I. L. Lagadic, M. K. Mitchell and B. D. Payne, *Environ. Sci. Technol.*, 2001, **35**, 984-990.
- 10 P. D. Cozzoli, R. Comparelli, E. Fanizza, M. L. Curri, A. Agostiano and D. Laub, *J. Am. Chem. Soc.*, 2004, **126**, 3868-3879.
- 11 X. C. Jiang, T. Herricks and Y. N. Xia, *Adv. Mater.*, 2003, **15**, 1205.
- 12 Y. L. Li and T. Ishigaki, *Chem. Mater.*, 2001, **13**, 1577-1584.
- 13 J. S. Chen, Y. L. Tan, C. M. Li, Y. L. Cheah, D. Luan, S. Madhavi, F. Y. C. Boey, L. A. Archer and X. W. Lou, *J. Am. Chem. Soc.*, 2010, **132**, 6124-6130.
- 14 D. Li and Y. N. Xia, *Nano Lett.*, 2003, **3**, 555-560.
- 15 Z. Miao, D. S. Xu, J. H. Ouyang, G. L. Guo, X. S. Zhao and Y. Q. Tang, *Nano Lett.*, 2002, **2**, 717-720.
- 16 H. B. Wu, H. H. Hng and X. W. Lou, *Adv. Mater.*, 2012, **24**, 2567-2571.
- 17 J. H. Lee, I. C. Leu, M. C. Hsu, Y. W. Chung and M. H. Hon, *J. Phys. Chem. B.*, 2005, **109**, 13056-13059.
- 18 K. Shankar, J. I. Basham, N. K. Allam, O. K. Varghese, G. K. Mor, X. J. Feng, M. Paulose, J. A. Seabold, K. S. Choi and C. A. Grimes, *J. Phys. Chem. C.*, 2009, **113**, 6327-59.
- 19 J. Wang and Z. Q. Lin, *Chem. Mater.*, 2008, **20**, 1257-1261.
- 20 W. T. Sun, Y. Yu, H. Y. Pan, X. F. Gao, Q. Chen and L. M. Peng, *J. Am. Chem. Soc.*, 2008, **130**, 1124-1125.
- 21 A. Goossens, E. L. Maloney and J. Schoonman, *Chem. Vapor Depos.*, 1998, **4**, 109-114.
- 22 L. L. Hench and J. K. West, *Chem. Rev.*, 1990, **90**, 33-72.
- 23 L. Spanhel and M. A. Anderson, *J. Am. Chem. Soc.*, 1991, **113**, 2826-2833.
- 24 J. P. Xie, Q. B. Zhang, J. Y. Lee, D. I. C. Wang, *ACS Nano*, 2008, **2**, 2473-2480.
- 25 B. Liu and H. C. Zeng, *J. Am. Chem. Soc.*, 2004, **126**, 16744-16746.
- 26 J. Q. Huang, Z. Huang, W. Guo, M. L. Wang, Y. G. Cao and M. C. Hong, *Cryst. Growth Des.*, 2008, **8**, 2444-2446.
- 27 J. Perlich, G. Kaune, M. Memesa, J. S. Gutmann and P. Muller-Buschbaum, *Philos. Trans. R. Soc. A.*, 2009, **367**, 1783-1798.
- 28 M. C. Lechmann, D. Kessler, J. S. Gutmann, *Langmuir*, 2009, **25**, 10202-10208.
- 29 B. Liu and H. C. Zeng, *J. Am. Chem. Soc.*, 2004, **126**, 8124-8125.
- 30 X. W. Lou, Y. Wang, C. Yuan, J. Y. Lee and L. A. Archer, *Adv. Mater.*, 2006, **18**, 2325-2329.
- 31 X. W. Lou and L. A. Archer, *Adv. Mater.*, 2008, **20**, 1853-1858.
- 32 R. L. Penn and J. F. Banfield, *Science*, 1998, **281**, 969-971.
- 33 R. L. Penn, *J. Phys. Chem. B.*, 2004, **108**, 12707-12712.
- 34 J. F. Zhu, W. Zheng, B. He, J. L. Zhang and M. Anpo, *J. Mol. Catal. A: Chem.*, 2004, **216**, 35-43.
- 35 B. Y. Xia, B. Wang, H. B. Wu, Z. Liu, X. Wang and X. W. Lou, *J. Mater. Chem.*, 2012, **22**, 16499-16505.
- 36 B. Y. Xia, Y. Yan, X. Wang and X. W. Lou, *Mater. Horiz.*, 2014.
- 37 M. Sevilla and A. B. Fuertes, *Energy Environ. Sci.*, 2011, **4**, 1765-1771.
- 38 A. Shabaev and A. L. Efros, *Nano Lett*, 2004, **4**, 1821-25.
- 39 Z. J. Gu, T. Y. Zhai, B. F. Gao, X. H. Sheng, Y. B. Wang, H. B. Fu, Y. Ma and J. N. Yao, *J. Phys. Chem. B.*, 2006, **110**, 23829-23836.
- 40 L. S. Zhang, W. Z. Wang, Z. G. Chen, L. Zhou, H. L. Xu and W. Zhu, *J. Mater. Chem.*, 2007, **17**, 2526-2532.
- 41 Z. Y. Liu, D. D. Sun, P. Guo and J. O. Leckie, *Chem. Eur. J.*, 2007, **13**, 1851-1855.
- 42 S. Musić, M. Gotić, M. Ivanda, S. Popović, A. Turković, R. Trojko, A. Sekulić and K. Furić, *Mater. Sci. Eng. B*, 1997, **47**, 33-40.
- 43 S. F. Wang, F. Gu, M. K. Lü, C. F. Song, S. W. Liu, D. Xu and D. R. Yuan, *Mater. Res. Bull.*, 2003, **38**, 1283-1288.
- 44 L. Hou, Y. D. Hou, M. K. Zhu, J. L. Tang, J. B. Liu, H. Wang and H. Yan, *Mater. Lett.*, 2005, **59**, 197-200.
- 45 B. Siemensemeyer and J. W. Schultze, *Surf. Interface Anal.*, 1990, **16**, 309-314.
- 46 B. S. Chiou and Y. J. Tsai, *J. Mater. Sci. Lett.*, 1989, **8**, 485-489.
- 47 Y. H. Ni, L. N. J, L. Z and J. M. H, *J. Mater. Chem.*, 2010, **20**, 6430-36.
- 48 L. Xiong, C. Chen, Q. Chen and J. Ni, *J. Hazard. Mater.*, 2011, **189**, 741-748.
- 49 Y. C. Chen, S. L. Lo and J. Kuo, *Colloids Surf. A.*, 2010, **361**, 126-131.
- 50 Y. H. Li, J. Ding, Z. K. Luan, Z. C. Di, Y. F. Zhu, C. L. Xu, D. H. Wu and B. Q. Wei, *Carbon*, 2003, **41**, 2787-2792.
- 51 R. Leyva-Ramos, L. A. Bernal-Jacome and I. Acosta-Rodriguez, *Sep. Purif. Technol.*, 2005, **45**, 41-49.
- 52 T. S. Anirudhan and P. S. Suchithra, *Chem. Eng. J.*, 2010, **156**, 146-156.

100

Contents entry



Schematic diagram of Cd(II) adsorption by nanostructured TiO_2 particles.